

Hydrogen in α iron: modification of elastic properties and solubility in strain fields

D. Psiachos¹

¹*ICAMS, Ruhr-Universität Bochum, Bochum, Germany*

Abstract

The effect of interstitial hydrogen on the elastic properties of α -iron is investigated using *ab initio* density functional theory. We find that while the overall strength properties are reduced by H, the effects are mainly due to the resulting local volume expansion. We use these concentration-dependent elastic moduli to model the effects of homogeneous strain fields on H solubility and make extrapolations to H-solubility in the spatially-varying strain fields of realistic dislocations. We find that H is strongly trapped by dislocations of both the edge and screw variety, leading to a remarkable increase in the local H concentration near the dislocation cores. The strain dependence of the solution energy leading to accumulation of H near dislocation cores, as well as the reduction of elastic moduli which our calculations predict, is consistent with numerous experimental studies which indicate that the trapping of H near dislocations plays a significant role in the embrittlement of iron and steels.

I. INTRODUCTION

Hydrogen degrades the performance of many metals by lowering the failure stress, leading to fracture at unpredictable loading conditions^{1,2}. Several mechanisms have been proposed to explain the H-embrittlement of iron: the hydrogen-enhanced decohesion (HEDE) mechanism^{3,4}, H-vacancy effects⁵⁻⁷, hydrogen-enhanced localised plasticity (HELP)⁸⁻¹⁰, or a combination thereof. However, none of these explanations alone seems to provide a complete explanation of the experimentally-observed features of H-embrittlement.

In the HEDE mechanism, H weakens the cohesive bonds between the metal atoms, leading to failure at interfaces, as H exhibits increased solubility in the tensile strain field of a crack opening. Vacancies containing H can order themselves along critical slip directions, leading to fracture^{6,7}. Within the HELP mechanism, the onset of plasticity with loading occurs at a lower stress as a result of the H shielding of repulsive interactions between dislocations⁹. The increased H concentration at dislocations¹¹ effectively reduces the dislocation-dislocation distances. Together with the experimentally-observed increase of dislocation mobility¹⁰, this may explain the phenomenon of dislocation coalescence, and ultimately, crack advancement at reduced loads. The importance of increased H-concentration near dislocations and other low-energy trap sites was also indicated by in a recent experimental study of intergranular failure in steel¹². In that study, the fracture mode changed from ductile to brittle, as the amount of H located at these low-energy trap sites increased, indicating that a study of H at dislocations is important.

The goal of this study is to achieve a microscopic understanding of the changes in the mechanical properties due to H, and their connection with the proposed theories of H-embrittlement. Focussing on α -Fe, we study the influence of interstitial H on the elastic properties, and the behaviour of H within strain fields representative of dislocations. To achieve this, we use density-functional theory (DFT) calculations to calculate the changes in the elastic properties of α - (bcc) iron, as a function of H-concentration and employ these results in a continuum elasticity theory description of the H-solubility in strain fields. In Sec. II we describe the details of our DFT calculations while Sec. III describes the calculations of the modification of the elastic parameters as a function of H-concentration. Sec. IV discusses the solubility of H in strain fields, and we conclude with a discussion in Sec. V.

II. DESCRIPTION OF FIRST-PRINCIPLES CALCULATIONS

Our first-principles density functional theory calculations were performed using the VASP¹³⁻¹⁵ code. We used the projector augmented-wave method^{16,17} and employed pseudopotentials considering the 3p electrons of Fe as valence electrons. The generalized-gradient approximation (GGA) in the PW91 parametrisation¹⁸ was used for the exchange-correlation functional. All of our calculations were spin-polarised. Some of our calculations were repeated using the Vosko-Wilk-Nusair¹⁹ (VWN) spin interpolation in PW91, or the Perdew-Burke-Ernzerhof²⁰ (PBE) exchange-correlation functional and are discussed in Sec. III D. A plane-wave basis with a cutoff of 500 eV and supercell geometry were used. A Γ -centred k-point grid equivalent to $18 \times 18 \times 18$ for the two-atom basis bcc unit cell was used for the Brillouin-zone sampling except for the 128-atom Fe cell where it was $20 \times 20 \times 20$. Our results for the lattice parameter (2.832 \AA), bulk modulus (194 GPa), and magnetic moment ($2.17 \mu_B$) are in good agreement with other first-principles calculations *e.g.* Refs. 21,22 and with experiment 23,24. The plane-wave basis and k-point sampling density used are more than adequate for converging the equilibrium properties, but necessary for converging elastic moduli to within less than one percent. The ions were relaxed such that the maximum component of the force on each ion was less than 0.01 eV/\AA while the total energies were converged to within 0.01 meV. The lattice parameter for systems constrained to be cubic (see following section for a discussion of this approximation) was determined from fitting the total energies to the Murnaghan equation of state²⁵. At times, the correct lattice parameters for a tetragonal unit cell were desired; these were obtained from a quadratic fit over a two-dimensional grid of total energies.

In this study, we focused our attention on tetrahedral interstitial H, for two reasons: one is that at zero stress we found the tetrahedral interstitial position to be 0.13 eV more stable than the octahedral position, in agreement with previous DFT studies^{26,27}, and secondly, as there are twice as many tetrahedral as octahedral sites per Fe atom (six versus three), we expect the former to dominate the mechanical properties at ambient temperatures.

III. ELASTIC PROPERTIES OF BCC-IRON

A. Calculation of elastic parameters

The total energy of a solid at zero stress and equilibrium volume V_0 can be expanded about small strains ϵ_m using the Voigt notation (m running from 1 to 6):

$$E(\epsilon) = E(0) + \frac{1}{2!}V_0 \sum_{ij} C_{ij}\epsilon_i\epsilon_j + \frac{1}{3!}V_0 \sum_{ijk} C_{ijk}\epsilon_i\epsilon_j\epsilon_k + \dots \quad (1)$$

In this section we restrict ourselves to linear elastic behaviour, *i.e.* stress linear in the strain the first two terms of Eq. 1. For the calculation of the elastic parameters in this work, cubic symmetry was enforced. This resulted in an error of less than 2%, as will be described at the end of this section. The number of independent elastic parameters C_{ij} depends on the crystallographic symmetry. For cubic systems, there are three unique elastic parameters, C_{11} , C_{12} , and C_{44} , that describe the change in energy due to applied strain. The parameters C_{ij} can be determined by applying suitable strain tensors and taking the second derivative of Eq. 1 with respect to the amount of strain. The combination $B = \frac{1}{3}(C_{11} + 2C_{12})$ is the bulk modulus, found by applying hydrostatic strains and then doing a fit to the Murnaghan equation of state, whereupon the pressure derivative $B'(P)$ is also found. The combination $C' = C_{11} - C_{12}$, and the coefficient C_{44} are found by applying volume-conserving strains.

In the case of C' , an orthorhombic strain

$$\epsilon = \begin{pmatrix} \delta & 0 & 0 \\ 0 & -\delta & 0 \\ 0 & 0 & \delta^2/(1 - \delta^2) \end{pmatrix} \quad (2)$$

is applied, giving a total energy expression

$$E_{ortho.}(\delta) = E(0) + C'V\delta^2 + O[\delta^4], \quad (3)$$

while, for C_{44} , the strain is monoclinic:

$$\epsilon = \begin{pmatrix} 0 & \delta/2 & 0 \\ \delta/2 & 0 & 0 \\ 0 & 0 & \delta^2/(4 - \delta^2) \end{pmatrix}. \quad (4)$$

with a total energy

$$E_{mono.}(\delta) = E(0) + \frac{1}{2}C_{44}V\delta^2 + O[\delta^4]. \quad (5)$$

We fitted our total energies for systems subject to nine values of strains δ between $\pm 3\%$ to Eqs. 3 and 5 in order to obtain C' and C_{44} . To estimate the accuracy of the elastic-parameter calculations, extensive convergence tests were done. The quantities varied were the k-point density, cutoff energy, and percent strain (value of δ). The lattice parameter was fixed at 2.832 Å for all tests. An example of these convergence tests for C_{44} is shown in Fig.1a, for $\delta=3\%$ (the convergence tests for C' are similar). The values of cutoff energy and k-point density of the circled point (500 eV, $18 \times 18 \times 18$) were used in (b) and (c) to check that the applied strains are within the linear regime. As a result of our extensive

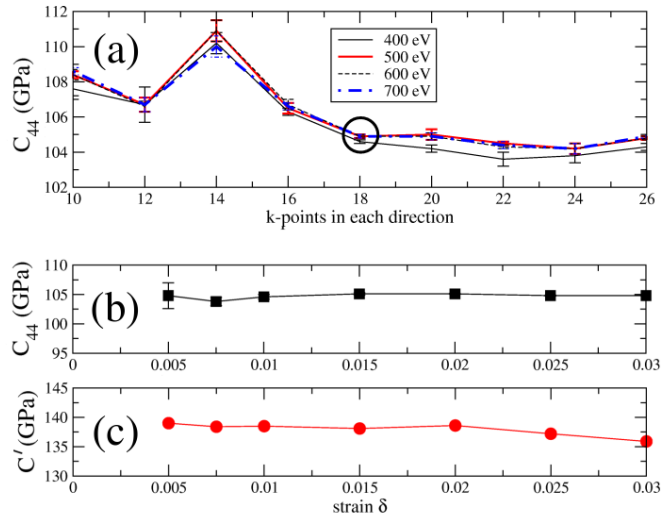


FIG. 1: (a) Convergence of C_{44} as a function of k-point density and energy cutoff for the two-atom bcc-Fe cell for a range of $|\delta| \leq 3\%$. The error bars are deduced from the least-squares fit to Eq. 5. The circled point corresponds to the calculational parameters used in this study. (b) C_{44} and (c) C' fitted between different ranges of $\pm\delta$.

convergence tests, we observed less than a 1% variation in the elastic parameters upon going from 0.5-3% change in δ . For the calculations presented in the remainder of this study, we chose a value of 3% for δ in order to avoid numerical instabilities and/or the need for very high precision total energy evaluations.

B. Elastic parameters of FeH

The volume expansion of the crystal lattice by H in the tetrahedral interstitial site introduces small tetragonal distortions, breaking the cubic symmetry of the Fe host lattice.

An H-orientation such as the one shown in Fig. 2 causes an expansion of the Fe nearest-neighbours radially-outward from H (along the red lines) This expansion, projected onto the cube axes, is of an identical amount in the a and c direction, and greater than the expansion along b . The tetragonal distortion, with lattice parameters $a = c \neq b$, increases the number

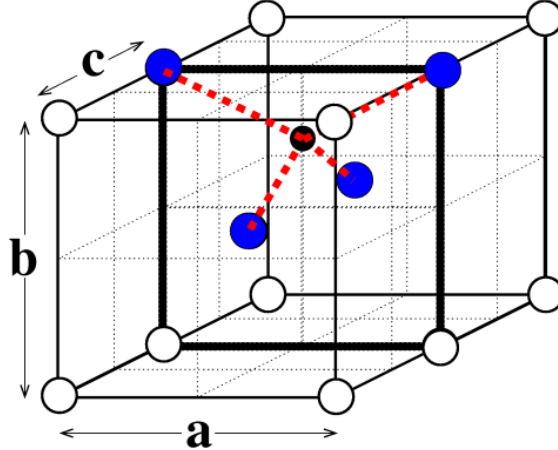


FIG. 2: Location of a H-interstitial on the face between two bcc unit cells. Lines towards nearest-Fe neighbours (blue circles) are shown.

of unique elastic parameters from three to six: $C_{12} = C_{23} \neq C_{13}$, $C_{11} = C_{33} \neq C_{22}$, and $C_{44} = C_{66} \neq C_{55}$. The variation among the no-longer equivalent elastic parameters depends on the degree of tetragonal distortion, generally becoming more pronounced with increasing H-concentration, unless there are two or more H in the supercell, in which case the amount of distortion depends also on their relative positions. Generally, H would be expected to be randomly distributed, resulting an isotropic lattice distortion. As well, considering a cubic unit cell facilitates the scale-bridging with mesoscopic approaches such as *e.g.* finite-element schemes.

The error due to imposing cubic symmetry can be estimated by explicitly calculating the (formally-degenerate in cubic symmetry) elastic parameters, for tetragonal symmetry for a configuration with lattice parameters $a = c \neq b$ by straining the system in all three cartesian orientations, all the while maintaining a cubic unit cell. The reason that the results are not equivalent in all directions even under the assumption of cubic symmetry is because of the local internal tetragonal symmetry around the H atom. Nevertheless, the variation amongst the three orientations was found to be small: in two of the orientations the elastic parameters were identical, as expected, while those from the third differed by about 4%,

making the standard error less than 2% for the highest concentration (11%) studied, where the tetragonal distortion $1 - b/a$ was -0.004, where the two H were oriented such that the distortion is double that caused by a single H. For all of our data above and including a H-concentration of 4%, the formally-degenerate elastic parameters were explicitly calculated by straining in the three cartesian directions and the results presented are the average values along with the associated standard errors. For lower concentrations, the spread amongst the three directions was $< 1\%$ and corresponding errors presented are from the least-squares fitting of the total energy as a function of strain.

In addition, for the system with $1 - b/a = -0.004$ (at 11 at.% H), the elastic parameters for an explicitly tetragonal lattice were calculated using the strain and total energy expressions given in Ref. 28. The differences from the simplified case of the cubic unit cell with distortions applied in all three orientations were small, less than 2% for the largest H-concentration studied. Table I summarises the average values of the cubic and tetragonal elastic parameters along with the associated standard errors computed from the spread in the values for the different orientations. Only \bar{C}_{12} gave a large spread for the tetragonal cell (separately, the values were $C_{12} = C_{23}=1.38$, $C_{13}=1.64$). That the agreement is good is not surprising, since the volume of the cubic cell was made to be the same as that of the tetragonal cell and the variation in the elastic parameters arising from different lattice parameters (Sec. III C) in the tetragonal cell mostly averages out in the cubic cell.

	cubic	tetragonal
$\bar{C}_{11} = \frac{1}{3} (C_{11} + C_{22} + C_{33})$	245±2	239±6
$\bar{C}_{12} = \frac{1}{3} (C_{12} + C_{13} + C_{23})$	142±2	147±15
$\bar{C}_{44} = \frac{1}{3} (C_{44} + C_{55} + C_{66})$	92±2	93±2

TABLE I: Elastic parameters (GPa) for the highest-considered H-concentration (11 at.%) for a cubic or tetragonal ($1-b/a=-0.4\%$) unit cell, both having the same volume. For the cubic cell, the strains were still performed in the three, formally-degenerate directions, and averaged, as the results were different due to the lower symmetry locally around the defect.

C. Non-linear elastic behaviour of pure Fe

In order to achieve a comprehensive description of the influence of volume-expansion due to interstitial H, we also investigated the nonlinear elastic behaviour of the elastic parameters as a function of hydrostatic strain. Equivalently, this is the effect of a volume expansion on the linear elastic parameters C_{ij} . The modified second-order elastic parameters are given by Birch²⁹ in terms of the second and third-order elastic parameters C_{ij} and C_{ijk} to linear order in the applied hydrostatic strain. Instead of calculating the third-order elastic parameters, we directly determined the variation in the second-order elastic parameters as a function of small applied hydrostatic strain such that the assumption of linear elasticity remains valid.

Following Wallace [30], the total energy at a volume V produced by strains applied at a reference volume V^{ref} away from equilibrium, is modified from Eq. 1 to include a term first-order in strain, corresponding to hydrostatic stress σ_{ij} :

$$E(V, \epsilon) = E(V^{ref}, \epsilon = 0) + V^{ref} \sum_{ij} \sigma_{ij} \epsilon_{ij} + \frac{V^{ref}}{2} \sum_{ijkl} C_{ijkl}(V^{ref}) \epsilon_{ij} \epsilon_{kl}. \quad (6)$$

In Eq. 6, (as in Eq. 2.37 in [30]) the strains are infinitesimal strains evaluated with respect to V^{ref} . Because the stress is hydrostatic, it can be written as $\sigma_{ij} = -P\delta_{ij}$. Expanding Eq. 6 and allowing the strains represented by Eq. 2 and 4 to be applied with respect to V^{ref} , we obtain the expressions, modified from those of Eq. 3 and 5,

$$E_{ortho.}(P, \delta) = E(P, 0) + (C' - P) V^{ref} \delta^2 + O[\delta^4], \quad (7)$$

$$E_{mono.}(P, \delta) = E(P, 0) + \frac{1}{2} \left(C_{44} - \frac{P}{2} \right) V^{ref} \delta^2 + O[\delta^4]. \quad (8)$$

At each value of η ranging between ± 0.05 , the value of δ was varied between ± 0.03 and a fit was made to second-order in δ , as in Sec. III A. The elastic parameters C' and C_{44} are again extracted from the coefficients of δ^2 . However, in order to separate C_{11} and C_{12} from C' , the bulk modulus needs to be adjusted to take into account the nonzero pressure, by an amount equal to its derivative found from the fit to the Murnaghan²⁵ equation of state (we found $B'(P) = 5.42$), multiplied by the pressure at the corresponding value of hydrostatic strain η . The variation of the elastic parameters with hydrostatic strain follows a linear trend, as can be seen from Fig.3. A linear least-squares fit to the small-strain region ($|\eta| < 0.02$) of these curves resulted in the following dependence of the elastic parameters on hydrostatic

strain:

$$\begin{aligned}
 B &= (194 - 1061\eta) \text{ GPa} \\
 C_{11} &= (284 - 1640\eta) \text{ GPa} \\
 C_{12} &= (149 - 798\eta) \text{ GPa} \\
 C_{44} &= (105 - 771\eta) \text{ GPa}
 \end{aligned} \tag{9}$$

Previously-reported first-principles calculations of the elastic parameters of bcc-Fe³¹⁻³³ show a spread of approximately 10%. Some of these results, including dependences on hydrostatic strain, if reported, along with values from an experiment performed at 4 Kelvin, are shown in Table II along with our results. We did a fit of the others' data to obtain the reference values listed in the table. The experimental data for the hydrostatic-strain dependences of the elastic parameters is sparse. The few experimental data points existing in the literature are superimposed onto the calculated results by Sha and Cohen³¹ in their paper, and these agree well with their calculations. Our derivatives do not deviate appreciably compared to the others' results.

method	C_{11} (GPa)	C_{12} (GPa)	C_{44} (GPa)
PAW-GGA (present)	284(-1640)	149(-798)	105(-771)
LMTO-GGA ³¹	303(-1282)	150(-813)	126(-604)
PAW-GGA ³²	271(-1228)	145(-535)	101(-454)
PP-GGA ³³	289	118	115
FP-LAPW ³⁴	285	139	100
expt. ²³	245	139	122
expt. ³⁵	240	136	121

TABLE II: Comparison of elastic parameters (and their hydrostatic strain η dependence in parentheses, if available) obtained in the present study with other calculations and experimental results.

D. Dependence of elastic parameters on H-concentration

The elastic parameters of pure Fe serve as a starting point for determining the influence of interstitial H atoms on the elastic properties. We implement the variation of H-concentration

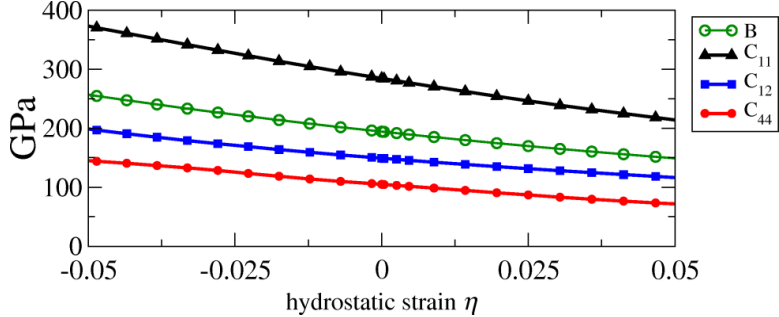


FIG. 3: Calculated elastic parameters for pure Fe as a function of applied hydrostatic strain $\eta \equiv \Delta V/V_0$ where V_0 is the equilibrium volume of bcc-Fe.

in the supercell approach of our calculations by (i) increasing the size of a supercell containing one H atom, or by (ii) adding a second H atom to the same supercell. In addition, we changed the symmetry of the supercell or the position of the second H atom relative to the first in order to alter the ordering of the H atoms within the Fe host lattice. The sizes of supercells and number of H atoms used to achieve various H concentrations are listed in Table III.

Figure 4 shows the variation with concentration of the elastic parameters. Additional data points at the same concentration correspond to differently-ordered structures (see Table III). There is a clear trend of decreasing elastic parameters with concentration. We fit a line to each set of data, which we will make use of in Sec. IV. This line was made to include the zero-concentration value and excluded the outliers at 0.8% and 10%. We ascribe the outlying values of C_{11} and C_{12} for the 10% concentration to the fact that this supercell had the largest stress associated with it. This was the case because of the relative orientation with which the two H atoms were set up, and also to the proximity to the periodic H images in the smallest dimension. The C_{44} at 0.8% (and to a lesser degree at 2.7%) lies outside the line of best fit and warrants further investigation as to whether it is a function of the precision used in the calculation or a genuine effect. We also repeated some of these calculations using the VWN corrections, and also with the PBE functional. They resulted in slightly different equilibrium lattice parameters (order of 0.3%), and correspondingly, different absolute moduli, but the slope of the C_{ij} versus concentration remained the same.

Calculations of the modification of elastic parameters of Fe by H has been reported recently in Ref. 36. Their underlying lattice was not perfect Fe but a crack with tens of thousands of atoms and an atomistic model was used for the calculations. The data covered

at. % H	n(H)	k×l×m
0	0	1×1×1
0.8	1	4×4×4
1.8	1	3×3×3
2.7	1	3×3×2
3.6	2	3×3×3
4.0	1	2×2×3
5.3	1	3×3×1
5.9	1	2×2×2
5.9	1	2×4×1
7.7	1	1×2×3
10.0	2	3×3×1
11.1	2	2×2×2

TABLE III: H-concentrations and how they were achieved based upon the number $n(\text{H})$ of H and supercell dimensions in multiples k , l , and m of the lattice parameters of the two-atom bcc Fe cell. For the highest concentration (11.1%), three configurations, with H-H spacings within the same supercell of 4.98, 3.66, and 2.31 Å were calculated.

up to 6 at.% H and while the elastic parameters decreased with H initially, the effect levelled off with increasing H and generally was far weaker than here.

Figure 5 shows that the volume of the supercell changed linearly with H concentration, and we fit a line through this data. These volume changes may be related to the strain parameter η of Fig.3, and Eqs. 9 to assign the changes in the elastic parameters as arising from volumetric effects or other effects.

The volume-induced changes in elastic properties are shown, together with the total effects originally displayed in Fig. 4, in Figure 6.

Single-crystal Fe samples with H are difficult to prepare while the measurements of the C_{ij} do not directly relate to the strength properties of the material. Most often, the samples are polycrystalline, and the usual measurements performed are those directly related to stiffness, tensile strength, and hardness, in other words the bulk, Young's and shear moduli. In addition, for higher-length-scale simulations such as finite-element calculations of realistic

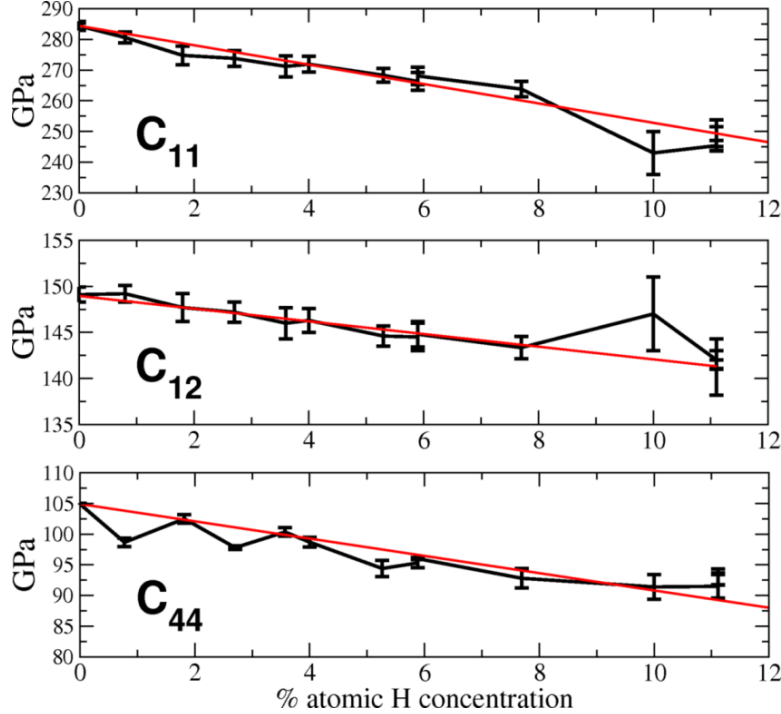


FIG. 4: Calculated elastic parameters for bcc Fe as a function of H concentration.

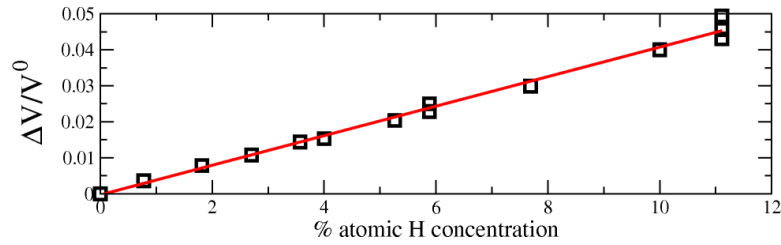


FIG. 5: Relative volume expansion as a function of H concentration where ΔV is the volume difference of the system with H compared with the pure Fe volume V^0 .

materials, the polycrystalline quantities are more practical than the single-crystal ones. Motivated by this, we used combinations of the elastic parameters C_{ij} , to derive various elastic moduli, describing different types of stress-strain responses. Shown in Fig. 7 are the bulk modulus, and the polycrystalline averages of the Young’s and shear moduli, where the average was performed according to the expression by Hill, which is an average of the Voigt and Reuss bounds³⁷. As in Fig. 6, the volumetric-strain-induced changes in the moduli for pure Fe are also shown.

The literature is extremely scarce on relevant measurements of elastic moduli of Fe with H. A rare exception is Ref. 38 where the effect of H on the shear modulus of polycrystalline

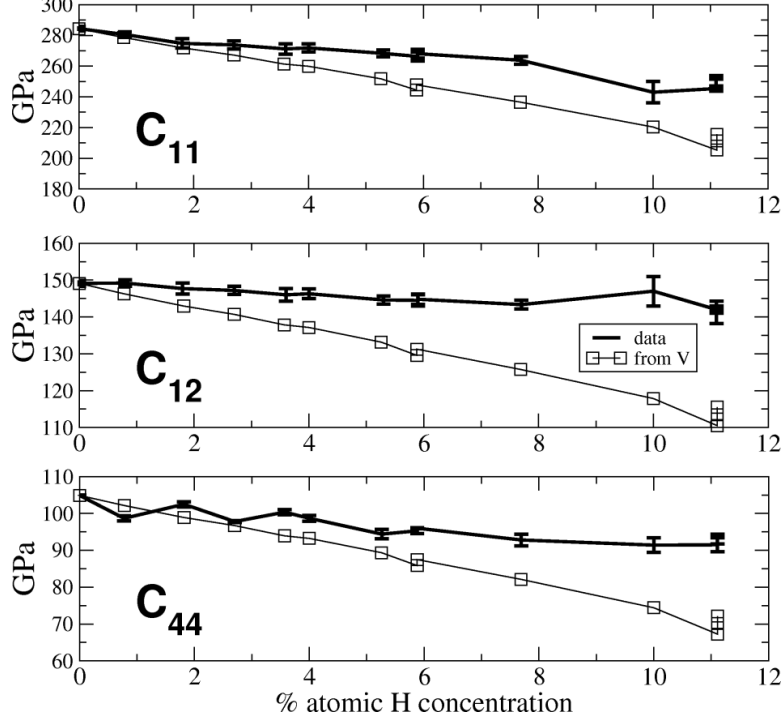


FIG. 6: Variation of elastic parameters from dft and from volume dependence of pure iron's elastic parameters

Fe was studied. They extrapolate their results to 1 at.% H and predict a decrease of 8% in the shear modulus at a temperature of 100 K, in agreement with our calculations.

By taking the difference of the two curves in Fig. 6 or Fig. 7, we remove the contribution of strain of pure Fe from the elastic parameters calculated at the equilibrium volume corresponding to each concentration of H. The resulting graphs, in Fig. 8, show only the electronic effect of H at each concentration (and implicit corresponding volume). These graphs show a clear trend in the elastic regime towards a stiffening, tensile strengthening, and hardening of the system with increasing concentration of H. Despite the overall softening of the material with increasing concentration, it is clear, that the effect of H leads to less softening than would be expected from the volume expansion alone. The separation of solute effects on the matrix elastic moduli has been also considered in Ref. 39 for H in Nb. Instead of parametrising the volume effect by the second term of their Eq. 4, we explicitly calculated it. Otherwise it's a straight line passing through our volume-derived elastic moduli curves. Similar analysis was done in Ref. 40.

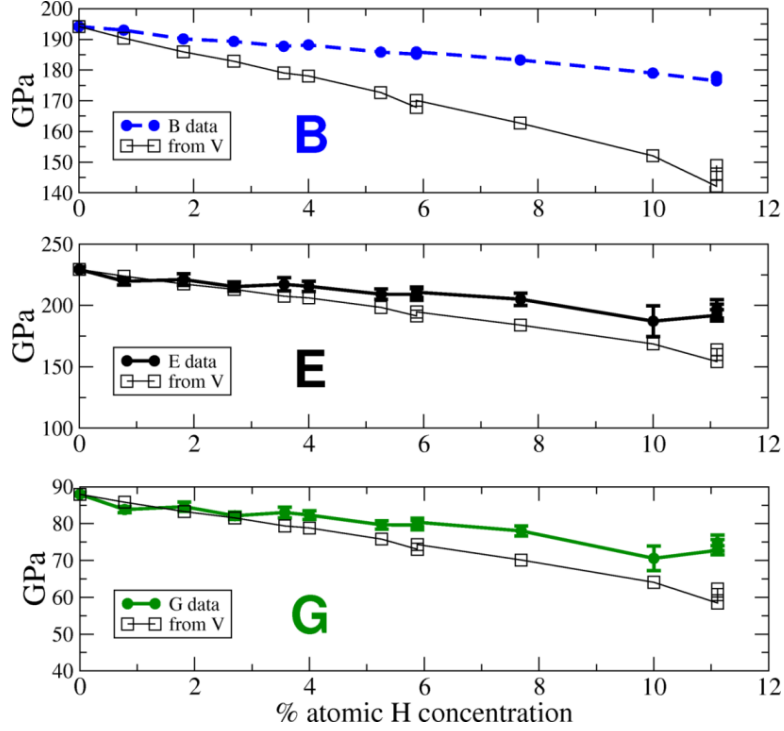


FIG. 7: Variation of polycrystalline moduli from DFT data (Fig. 4), and from the volume dependence of pure iron's elastic parameters

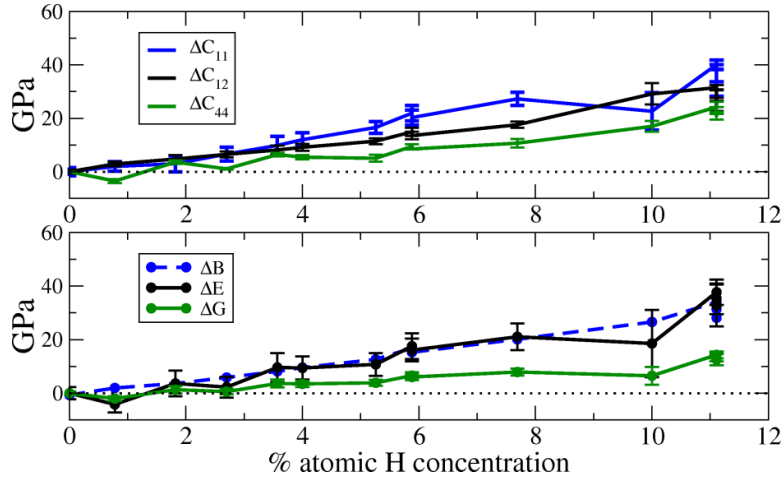


FIG. 8: Removal of volume-dependence of elastic moduli (subtracting DFT data from V-dependence in Figs. 6-7).

IV. STRAIN-DEPENDENCE OF H SOLUBILITY

In this section, we describe the effect of different types of strain on H solubility. Our goal is to examine the effect of H on typical dislocation strain fields and conversely, the latter's

impact on H solubility. In order to avoid the computationally very demanding explicit treatment of dislocations in correspondingly large supercells, we have instead examined the solubility of H in different types of homogeneous strain fields which we later used to estimate the H-solubility in realistic dislocation elastic strain fields.

Specifically, we have calculated the heats of solution for tetrahedral H in supercells subject to hydrostatic, or uniaxial or shear strain. These applied strain tensors mimic the strain fields of different dislocations as discussed in detail below.

To arrive at the heat of solution, W , at each value of applied strain, we subtracted from the total energy of the cell with N Fe atoms and n H atoms, E_{FeH_n} , the total energy E_{Fe} of a pure iron cell with N Fe atoms, and half the energy of a free H_2 molecule multiplied by n :

$$W(n) = E_{FeH_n} - E_{Fe} - n \frac{1}{2} E_{H_2}. \quad (10)$$

In all calculations, the cells with H were constrained to be cubic in their unstrained state, which is a good approximation, as described earlier, in Sec. III B.

Equation 10, however, can be interpreted in different ways depending on the strain or stress state of the pure Fe reference system with respect to the system with H. Therefore, as the definition of solution energy is ambiguous, we have defined four regimes on which to concentrate as the strain of the FeH system is varied: (i) one where the pure Fe volume matches that of the FeH system at each strain, (ii) where the two systems have the same stress tensor at each strain, and (iii) where they have the same strain tensors.

A. Parametrisation of the H-solution energy

Using our DFT-obtained material parameters (Table IV), we have parametrised the solution energies (Eq. 10) as functions of strain and H-concentration and we find them to accurately describe our DFT results, to a large extent quantitatively. We label all quantities with an x or 0 superscript for the FeH or pure Fe system respectively to denote which system they correspond to, for example, V^x for the equilibrium volume of the FeH system and V^0 for that of pure Fe. For a system Y ($=0$ for Fe, x for FeH), the total energy at an arbitrary reference volume V^{ref} and infinitesimal strain tensor ϵ with respect to V^{ref} is (*c.f.* Eq. 6)

$$E^Y(V^{ref}, \epsilon) = E^Y(V^{ref}, 0) + V^{ref} \sum_{ij} \sigma_{ij}^Y \epsilon_{ij} + \frac{V^{ref}}{2} \sum_{ijkl} C_{ijkl}^Y(V^{ref}) \epsilon_{ij} \epsilon_{kl}, \quad (11)$$

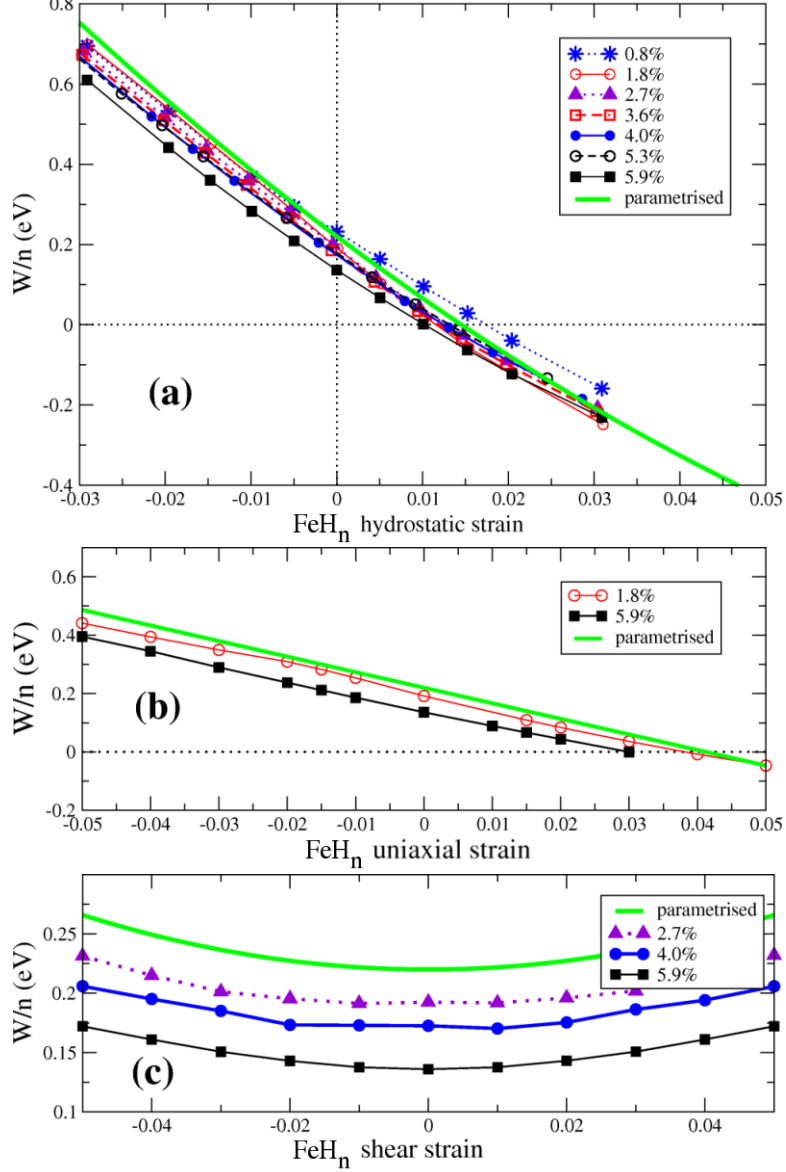


FIG. 9: DFT-calculated solution energies along with parametrised form for (a) hydrostatic strain, (b) uniaxial strain, (c) shear strain, for different H-concentrations.

where the first term is the total energy at the reference volume V^{ref} , the second term is the stress part which is non-zero if V^{ref} is not the equilibrium volume V^Y of Y , and the last term is the elastic deformation energy about V^{ref} . Explicitly, the first term is equal to

$$\begin{aligned}
 E^Y(V^{ref}, 0) &= E^Y(V^Y, 0) + \frac{1}{2} (V^{ref} - V^Y)^2 \left. \frac{\partial^2 E^Y}{\partial V^2} \right|_{V=V^Y} \\
 &= E^Y(V^Y, 0) + \frac{B^Y}{2V^Y} (V^{ref} - V^Y)^2,
 \end{aligned} \tag{12}$$

where B^Y is the bulk modulus of Y at V^Y . The second term, assuming a hydrostatic stress corresponding to a pressure P^Y to achieve the reference volume is

$$\begin{aligned}
V^{ref} \sum_{ij} \sigma_{ij}^Y \epsilon_{ij} &= -P^Y V^{ref} \sum_{ij} \delta_{ij} \epsilon_{ij} \\
&= -P^Y V^{ref} \sum_i \epsilon_{ii} \\
&= \frac{B^Y V^{ref}}{V^Y} (V^{ref} - V^Y) \sum_i \epsilon_{ii},
\end{aligned} \tag{13}$$

where the relation $P^Y = -B^Y (V^{ref} - V^Y) / V^Y$ has been used. This relation for P^Y assumes linear elasticity holds (B^Y doesn't vary) but the contribution of Eq. 13 is of $O(x^2)$ and as such this assumption is reasonable for low concentrations. In the third term of Eq. 11, the elastic parameters are evaluated at the volume V^{ref} and as such, they are equal to

$$\begin{aligned}
C_{ijkl}^Y(V^{ref}) &= C_{ijkl}^Y(V^Y) + \left. \frac{\partial C_{ijkl}^Y}{\partial V} \right|_{V=V^Y} (V^{ref} - V^Y) \\
&= C_{ijkl}^Y(V^Y) + \frac{1}{V^Y} \frac{\partial C_{ijkl}^Y}{\partial \eta} (V^{ref} - V^Y),
\end{aligned} \tag{14}$$

where the volume derivative has been rewritten in terms of the hydrostatic strain $\eta \equiv (V^{ref} - V^Y) / V^Y$. Despite their generality, Eqs. 12-14 are difficult to work with for the FeH system, as we do not have explicit data on the strain-dependence of the C_{ijkl}^Y . Therefore, when dealing with the FeH system, we take the reference volume as $V^{ref} = V^x$. The volume V^x may be expanded about V^0 , for small x as $V^x = V^0 + x dV/dx$.

We now list the expressions pertaining to FeH. These will remain the same throughout for all applications considered. The first term of Eq. 11 (*i.e.* Eq. 12) is equal to

$$\begin{aligned}
E^x(V^x, 0) &= E^0(V^0, 0) + x \left. \frac{\partial E}{\partial x} \right|_{V^0, x=0} + x (V^x - V^0) \left. \frac{\partial^2 E}{\partial x \partial V} \right|_{V^0, x=0} \\
&+ \frac{1}{2} (V^x - V^0)^2 \left. \frac{\partial^2 E}{\partial V^2} \right|_{V^0, x=0} + \frac{1}{2} x^2 \left. \frac{\partial^2 E}{\partial x^2} \right|_{V^0, x=0} \\
&= E^0 + x \frac{\partial E}{\partial x} + x^2 \frac{dV}{dx} \frac{\partial^2 E}{\partial x \partial V} + \frac{B^0}{2V^0} \left(x \frac{dV}{dx} \right)^2 + \frac{1}{2} x^2 \frac{\partial^2 E}{\partial x^2},
\end{aligned} \tag{15}$$

where here and in what follows, the limits of evaluation of the derivatives are omitted for clarity. In Eq. 15, the first derivative with respect to volume does not appear because it is equal to zero as the evaluation limits pertain to pure Fe. The second term of Eq. 11 (*i.e.* Eq. 13) is zero because V^x is the system's equilibrium volume. For the third term, the

elastic parameters (Eq. 14) are

$$C_{ijkl}^x \equiv C_{ijkl}^x(V^x) = C_{ijkl}^0 + \frac{dC_{ijkl}^{tot}}{dx}x, \quad (16)$$

where the derivative represents the variation not only with respect to concentration about V^0 but with strain implicitly included as well. These derivatives are the slopes of the lines of best fit from Fig. 4.

After defining the relative volumes, stresses, and/or strains, of the FeH and Fe systems corresponding to each of the cases outlined above, we use Eqs. 11 and 10 to derive strain-dependent solution energies for different relative strain and/or volume conditions for the Fe and FeH systems.

1. same volumes

The case of equal volumes would reflect the energy to be gained or lost by inserting $\frac{1}{2}H_2$ into a strained Fe lattice without further changing the average volume per Fe atom. Since the reference volume of the FeH system is V^x , that is also the reference volume of the pure Fe system. This results in a contribution from Eq. 13. We choose the strains to be $\epsilon = \epsilon^x$, the FeH system strains. The pure Fe system, at a reference volume V^x , applying the equations of the previous section (Eq. 11 and following), is described by a total energy

$$E^0(V^x, \epsilon^x) = E^0 + \frac{B^0}{2V^0} \left(x \frac{dV}{dx} \right)^2 + B^0 x \frac{dV}{dx} \sum_i \epsilon_{ii}^x + \frac{V^x}{2} \sum_{ijkl} C_{ijkl}^0(V^x) \epsilon_{ij}^x \epsilon_{kl}^x \quad (17)$$

where the elastic parameters are, applying Eq. 14,

$$\begin{aligned} C_{ijkl}^0(V^x) &= C_{ijkl}^0(V^0) + \frac{1}{V^0} \frac{\partial C_{ijkl}^0}{\partial \eta} (V^x - V^0) \\ &= C_{ijkl}^0(V^0) + \frac{1}{V^0} \frac{\partial C_{ijkl}^0}{\partial \eta} x \frac{dV}{dx}. \end{aligned} \quad (18)$$

The solution energy, obtained by collecting all the contributions to Eq. 11 and then using Eq. 10, neglecting all terms of order x^2 except for those appearing in Eq. 15, because we want to explain only the discrepancies at zero strain between the various concentrations, is

Quantity	value
ΔE	0.22 eV
B^0	194.2 GPa
ΔV	4.5 Å ³
V^0/N	11.352 Å ³
$dB^0/d\eta$	-1061 GPa
$dC_{11}^0/d\eta$	-1508 GPa
$dC_{12}^0/d\eta$	-885 GPa
$dC_{44}^0/d\eta$	-677 GPa
dB^{tot}/dx	-153 GPa
dC_{11}^{tot}/dx	-316 GPa
dC_{12}^{tot}/dx	-72 GPa
dC_{44}^{tot}/dx	-141 GPa

TABLE IV: Parameters used in the expressions 19 - 23. Also used in subsequent sections. All derivatives are evaluated at V^0 and $x = 0$.

found for a cubic system to be equal to

$$\begin{aligned}
W/n &= \Delta E + \frac{x}{2N} \frac{\partial^2 E}{\partial x^2} + x \Delta V \frac{\partial^2 E}{\partial x \partial V} - B^0 \Delta V (\epsilon_{xx}^x + \epsilon_{yy}^x + \epsilon_{zz}^x) \\
&+ \frac{1}{2} \left[\left(\frac{V^0}{N} \frac{dC_{11}^{tot}}{dx} - \frac{dC_{11}^0}{d\eta} \Delta V \right) (\epsilon_{xx}^x{}^2 + \epsilon_{yy}^x{}^2 + \epsilon_{zz}^x{}^2) \right. \\
&+ 2 \left(\frac{V^0}{N} \frac{dC_{12}^{tot}}{dx} - \frac{dC_{12}^0}{d\eta} \Delta V \right) (\epsilon_{xx}^x \epsilon_{yy}^x + \epsilon_{xx}^x \epsilon_{zz}^x + \epsilon_{yy}^x \epsilon_{zz}^x) \\
&\left. + 4 \left(\frac{V^0}{N} \frac{dC_{44}^{tot}}{dx} - \frac{dC_{44}^0}{d\eta} \Delta V \right) (\epsilon_{xy}^x{}^2 + \epsilon_{xz}^x{}^2 + \epsilon_{yz}^x{}^2) \right]. \quad (19)
\end{aligned}$$

In the above, we have used the definition of concentration as the ratio of the number of H atoms, n , to the number of Fe atoms N : $x = n/N$, to rewrite the concentration derivative of V in terms of the volume expansion ΔV per H and N : $\frac{dV}{dx} = \frac{dV}{dn} \frac{dn}{dx} = \Delta V N$ and similarly for the concentration derivative of E , $\frac{dE}{dx} = \Delta E N$. The ratio V^0/N is the volume per Fe atom at equilibrium, a constant. Numerical values of all quantities appearing in the parametrisation are listed in Table IV. $\Delta E=0.22$ eV was obtained by calculating the $\frac{1}{2}H_2$ solution energy in the largest unit cell (128 atoms) studied. The parametrised curves in all of the figures were generated by assuming a vanishing concentration, such that the contribution from the

$x(\%)$	$\Delta E + \frac{x}{2N} \frac{d^2 E}{dx^2} (\text{eV})$	$x\Delta V \frac{\partial^2 E}{\partial x \partial V} (\text{eV})$	sum	DFT $W(x) _{\epsilon^x=0} (\text{eV})$
0.8	0.246	-0.023	0.223	0.229
1.8	0.238	-0.048	0.190	0.192
2.7	0.249	-0.066	0.183	0.190
3.6	0.251	-0.089	0.162	0.175
4.0	0.250	-0.093	0.157	0.173
5.3	0.278	-0.123	0.155	0.177
5.9	0.255	-0.149	0.106	0.136

TABLE V: Energy terms from Eq. 12 contributing to the intercept at zero strain for the case of equal volumes (Fig. 9). The first two energy columns are from expression 15 and were calculated using DFT as described in the text. Their sum is under the heading *sum*. The last column is the DFT data.

x -dependent parts of Eqs. 19 - 23 is zero.

For the case of hydrostatic strain $\epsilon = \epsilon_{xx} = \epsilon_{yy} = \epsilon_{zz}$, Eq. 19 becomes

$$W^{hydro}/n = \Delta E + \frac{x}{2N} \frac{\partial^2 E}{\partial x^2} + x\Delta V \frac{\partial^2 E}{\partial x \partial V} - 3B^0 \Delta V \epsilon + \frac{9}{2} \left(\frac{V^0}{N} \frac{dB^{tot}}{dx} - \frac{dB^0}{d\eta} \Delta V \right) \epsilon^2. \quad (20)$$

For uniaxial strain $\epsilon \equiv \epsilon_{xx}$ and shear strain $\epsilon \equiv \epsilon_{xy} = \epsilon_{yx}$ the resulting expressions had the form

$$W^{uniax.}/n = \Delta E + \frac{x}{2N} \frac{\partial^2 E}{\partial x^2} + x\Delta V \frac{\partial^2 E}{\partial x \partial V} - B^0 \Delta V \epsilon + \frac{1}{2} \left(\frac{V^0}{N} \frac{dC_{11}^{tot}}{dx} - \frac{dC_{11}^0}{d\eta} \Delta V \right) \epsilon^2 \quad (21)$$

$$W^{shear}/n = \Delta E + \frac{x}{2N} \frac{\partial^2 E}{\partial x^2} + x\Delta V \frac{\partial^2 E}{\partial x \partial V} + 2 \left(\frac{V^0}{N} \frac{dC_{44}^{tot}}{dx} - \frac{dC_{44}^0}{d\eta} \Delta V \right) \epsilon^2. \quad (22)$$

Having a combination of hydrostatic/uniaxial/shear strain would involve combining expressions 20-22 as can be seen from Eq. 19 in any case.

We performed DFT simulations with the Fe and FeH systems at the same volume and varied the amount and type of strain. We subtracted the two sets of energies and the energy of $\frac{1}{2}H_2$, as in Eq. 10. The parametrised forms (Eqs. 20-22), using the DFT-calculated parameters listed in Table IV, accurately describe the DFT-obtained solution energies, as can be seen from Figure 9. Minor variations are seen for the calculated solution energies at zero strain among the various concentrations, and this can be accounted for entirely by evaluating the terms $x \frac{\partial E}{\partial x} + x^2 \frac{dV}{dx} \frac{\partial^2 E}{\partial x \partial V} + \frac{1}{2} x^2 \frac{\partial^2 E}{\partial x^2}$ (*c.f.* Eq. 15 and the normalised form in

Eq. 19) explicitly at each concentration studied. The cross-term $\frac{\partial^2 E}{\partial x \partial V}$ was calculated at the point $x=1.8\%$ and this value ($-0.557 \text{ eV}/\text{\AA}$) was used throughout. Using a graph similar to Fig. 9a, but with the horizontal axis in terms of the strain ϵ^0 of pure Fe, $x\frac{\partial E}{\partial x} + \frac{1}{2}x^2\frac{\partial^2 E}{\partial x^2}$ was predicted using the zero-strain data (equal to a volume of V^0) from there. This can be done since $W(x)|_{\epsilon^0=0} = \Delta E + \frac{x}{2N}\frac{d^2 E}{dx^2}$. These are given in the Table V. The sum of these two terms, stated in the third column, agrees very well with the DFT data given in the last column. The cross-term was also calculated using data from the 5.9% concentration and it was a bit smaller ($-0.426 \text{ eV}/\text{\AA}$) than the one used for Table V, leading to a contribution $x^2\frac{dV}{dx}\frac{\partial^2 E}{\partial x \partial V} = -0.114 \text{ eV}$ and thus a total $E^x(V^x, 0) = 0.141 \text{ eV}$, at $x = 5.9\%$, thus accounting for the minor deviations at the higher concentrations between the two last columns of the table. The deviation of the intercept from the ideal value 0.22 eV for all the graphs shown in Fig. 9 can thus be explained.

A derivation of the solution energy as a function of strain and concentration was presented in Ref. 41. In that work, the authors presented a systematic expansion of the total energy in terms of strain and concentration. They find, as we do, that the derivative of pressure with respect to concentration yields a contribution to the solution energy that is linear in hydrostatic strain. Using their expressions to express our concentration and strain-dependent elastic parameters requires considering up to the third derivatives of the total energy with respect to concentration and strain, which is the same as our concentration and strain-dependent elastic parameters.

2. same stresses or same strains

Another possibility of evaluating the solution energy Eq. 10 is to compare the FeH and pure Fe reference systems with both having the same stress or strain tensors. We choose to therefore expand the total energy of each system about its equilibrium volume.

For the two systems to have the same stresses σ_n , we must have, in the Voigt notation,

$$\sigma_n = \sum_m C_{nm}^0 \epsilon_m^0 = \sum_k C_{nk}^x \epsilon_k^x$$

for m, n, k from 1 to 6. In the case of hydrostatic strain $\epsilon_{ij}^x = \delta_{ij}\epsilon$, this leads to $\epsilon_{ii}^0 = \epsilon\frac{B^x}{B^0}$. In the case of the systems instead having equal strain tensors, we simply have $\epsilon_{ij}^0 = \epsilon_{ij}^x$.

As in the previous example, we apply Eq. 15 and we obtain, as a function of FeH

hydrostatic strain $\epsilon_{ij}^x = \delta_{ij}\epsilon$ and shear strain $\epsilon_{xy}^x = \epsilon_{yx}^x = \delta$, the following expression for the solution energy per H:

$$W/n = \Delta E + \frac{x}{2N} \frac{\partial^2 E}{\partial x^2} + x\Delta V \frac{\partial^2 E}{\partial x \partial V} + \frac{B^0}{2} \frac{N}{V^0} x\Delta V^2 + \frac{9}{2} \left[B^0 \Delta V \pm \frac{V^0}{N} \frac{dB^{tot}}{dx} \right] \epsilon^2 + 2 \left[C_{44}^0 \Delta V \pm \frac{V^0}{N} \frac{dC_{44}^{tot}}{dx} \right] \delta^2. \quad (23)$$

The upper (lower) sign is for the case where the strains (stresses) are equal. Eq. 23 is sufficiently general such that expressions can be found for mixed cases, *e.g.* equal hydrostatic stresses but equal shear *strains*. The expression 23 is compared with DFT data in Figure 10. The case $\delta = 0$ and varying ϵ for equal strains is shown in (a) while (b) has equal strains as well but here $\epsilon = 0$ and δ varies. In (c) we compare the case of equal stresses for $\epsilon = 0$ and δ varying. All the parameters were taken from Table IV, and converted to eV/Å³ prior to using.

The higher curvature for the 2.7% concentration in (c) occurs because at this concentration, the C_{44} data (Fig. 4) lies below the line of best fit, thereby giving a larger contribution to the total derivative.

As with the previous case of equal volumes, the intercept at zero strain in Fig. 10 can be accounted for by explicitly calculating the zero-strain terms appearing in Eq. 23. The comparison, given in Table VI, is very good for small concentrations and deviates for the larger one, by a similar amount as the case of constant volumes. As in that case, discussed at the end of Sec. IV A 1, the deviation is attributed here as well to variation of the cross-term with concentration.

$x(\%)$	Table V sum	$\frac{B^0}{2} \frac{N}{V^0} x\Delta V^2$	sum	DFT $W(x) _{\epsilon^x=0}$ (eV)
2.7	0.183	0.030	0.213	0.220
4.0	0.157	0.045	0.202	0.211
5.9	0.106	0.068	0.174	0.202

TABLE VI: Energy terms contributing to the intercept at zero strain (Fig. 10) for the case of equal strains or stresses. The first energy column is the same as that in Table V while there is now an additional term (second energy column in this table) appearing. The sum of the first two columns is under the third column, *sum*, which should be compared with the DFT data in the last column.

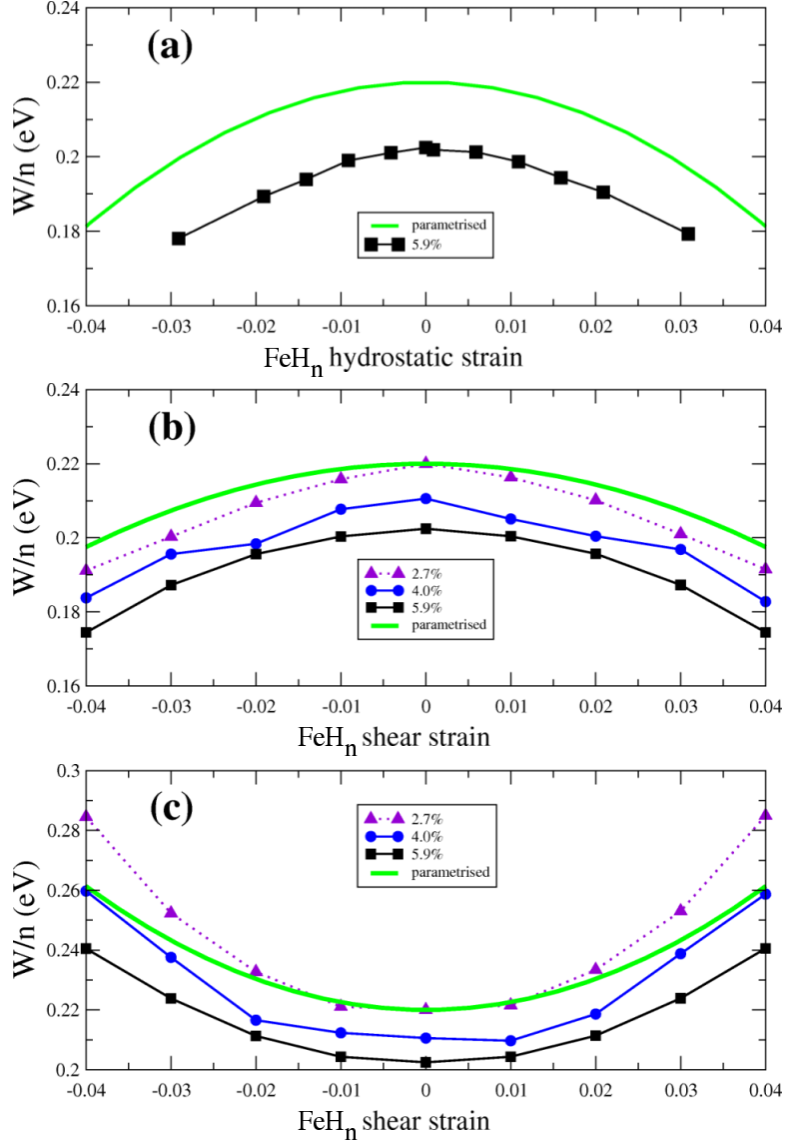


FIG. 10: DFT-calculated solution energies per H atom for various concentrations along with parametrised forms (Eq. 23) for a reference pure Fe system with (a) same strains, hydrostatic only (b) same strains, shear only, and (c) same stresses, shear only. The strain on the horizontal axis is for the FeH system.

B. H-solubilities in realistic dislocation strain fields

Here we will look at the variation of H-solubility as a function of strain direction. As well, we aim to visualise the H-solubility in a typical dislocation strain field. We will focus on the particular case of a screw dislocation lying along $\langle 111 \rangle$, which is the predominant orientation in a bcc metal⁴². The screw dislocation strain field was modelled using isotropic dislocation

theory⁴³. In cylindrical (r, θ, z) coordinates, its only nonzero component is $\epsilon_{\theta z} = \epsilon_{z\theta} = \frac{b}{4\pi r}$ where $b = 2.45\text{\AA}$ is a Burger's vector equal to the length of $\frac{1}{2}\langle 111 \rangle$.

All of the figures and equations for shear strain (Figs. 9c, 10b-c, Eqs. 22-23) look the same whether the shear strain is $\epsilon_{xy}^x = \epsilon_{yx}^x = \delta$, $\epsilon_{xz}^x = \epsilon_{zx}^x = \delta$, or $\epsilon_{yz}^x = \epsilon_{zy}^x = \delta$. For a screw dislocation line situated along $\langle 001 \rangle$, the nonzero components are $\epsilon_{xz}^x = \epsilon_{zx}^x = \epsilon_{yz}^x = \epsilon_{zy}^x = \delta$. Therefore, referring to Fig. 10, we see that H is trapped towards a screw dislocation core in the case where the pure Fe reference system has the same shear strain as the FeH system (Fig. 10b). We aimed to see whether the repulsive behaviour of H by a screw dislocation at constant volumes (Fig. 9c) can be altered, or even reversed in orientations other than the coordinate system defined by the cube axes.

The solubility equations 20-23 were examined to see whether they yield different values in rotated coordinates corresponding other orientations of the dislocation line. Depending on the choice of coordinate system, it is, in general, possible to get stronger or weaker variations for the solubility than those shown in Fig. 9. Already another combined atomistic/DFT study has shown that H-trapping in bcc Fe is very dependent to the direction of applied shear⁴⁴.

For the case of purely hydrostatic strain, we find that the solution energy was independent of the coordinate system chosen. This is because in our model (Eq. 19) both the term linear in strain as well as the quadratic term can be factored in terms of the trace $\epsilon_{xx} + \epsilon_{yy} + \epsilon_{zz}$. Since, as can be shown, the trace of the strain tensor is invariant under any unitary transformation, the solution energy for a hydrostatic distortion is thus rotationally-invariant. In the case of the screw dislocation, there is no such restriction; it is certainly possible to have different coefficients, some leading to H-trapping near a screw dislocation core.

Figure 11 shows the variation of the solution energy for a fixed, 2%, shear strain where Eq. 22 has been rotated onto other axes. By rotating the entire coordinate system, $(x, y, z) \rightarrow (x', y', z')$, other directions z' for the dislocation line (legend labels) are achieved. The label θ on the horizontal scale defines y' and hence the shear direction. As the directions $\langle 1\bar{1}0 \rangle$, $\langle 11\bar{2} \rangle$, and $\langle 111 \rangle$ are mutually perpendicular, the first two intersect the latter at $\theta \approx 35^\circ$ and $\theta = \pi/2$ respectively. We expressed the strains $\epsilon_{x'z'} = \epsilon_{z'x'}$ in the primed system in terms of the unprimed system and inserted these values into the general expression for the solution energy Eq. 19. Note that only the $\epsilon_{x'z'}^x = \epsilon_{z'x'}^x$ components are considered. For the full description of the screw dislocation, the $\epsilon_{y'z'}^x = \epsilon_{z'y'}^x$ components are also active. The

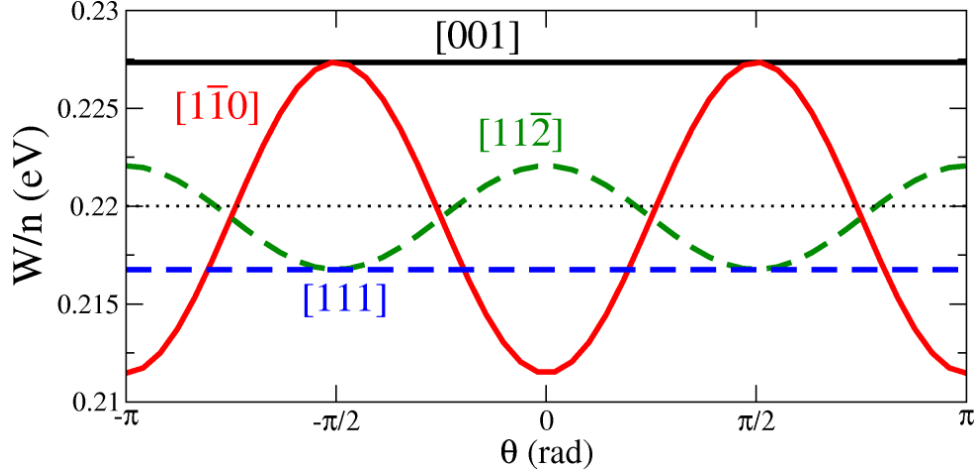


FIG. 11: Variation of solution energy for 2% shear strain (Eq. 22) for a dislocation line/Burger's vector oriented along different directions (legend). The direction of the dislocation line/ Burger's vector is, black: [001], blue dashed: [111], red: $[1\bar{1}0]$, green dashed $[11\bar{2}]$. The horizontal axis is the variation of the solution energy as a function of the choice of x' and y' axes (and hence the shear) within the plane normal to the Burger's vector. $\theta = 0$ has been arbitrarily chosen to correspond to the $y' = \langle \bar{k}h0 \rangle$ direction. The dotted line is the unstrained value of the H solution energy.

latter components result in the same curves as those depicted except with a $\pi/2$ phase shift such that the average value, corresponding to all components of a screw dislocation, is flat, independent of shear direction. In contrast with the study [44], we do not find asymmetry of our solution energy W about zero strain as a function of applied shear strain. To do otherwise would mean acquiring linear terms, which are not possible with our model.

For each point on a grid in the plane perpendicular to the dislocation line, the solubility corresponding to the complete strain tensor was calculated from Eq. 19 in the case of equal volumes or analogous equations (not given due to their complexity) for the cases of equal stresses and equal strain. One caveat concerning the case of equal stresses is that we are not modelling the solubility of H in the stress field of a dislocation but its solubility at individual stresses at each point r , such that the material is not self-consistently in mechanical equilibrium. However, this is a first approximation in a self-consistent treatment of H-solubility 45. The results, shown in Fig. 12, show that H is attracted to the core for equal shear strains or equal volumes and repelled for equal shear stresses.

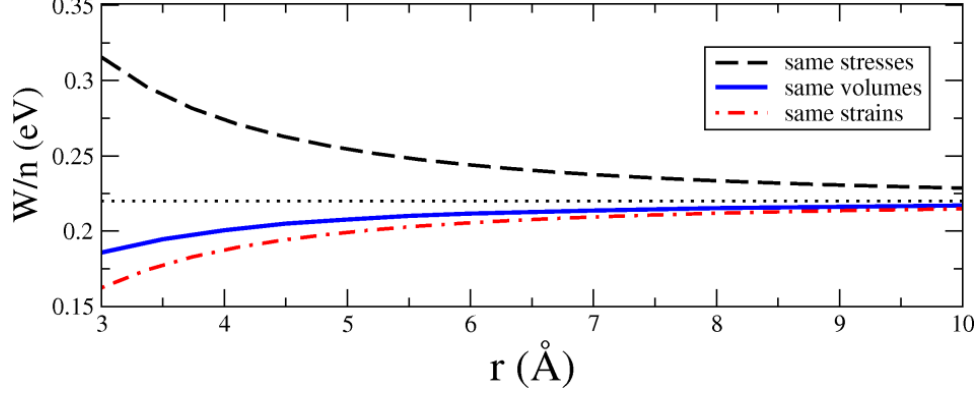


FIG. 12: Variation of H-solubility energy as a function of distance from the $\langle 111 \rangle$ screw dislocation core for the cases of equal stresses, equal volume, or equal strains for the FeH and pure Fe systems. The dotted line denotes the zero-strain solubility.

C. Concentration of H around strain fields

Motivated by the strong strain-solubility effects, we aim to calculate the local modification of the H concentration by strain fields. For the purposes of illustration, we consider only the case of equal volumes in this discussion. We consider the change in free energy F as a result of adding H to Fe under strain. The free energy is

$$F = E_{FeH} - TS, \quad (24)$$

where T is the temperature, and S is the total entropy of the FeH system. In order to isolate the effect of adding H to the already-strained Fe lattice, we assume that the entropy of the H is independent of that of the Fe lattice: *i.e.* $S = S_H + S_{Fe}$. E_{FeH} is the total energy of the (strained) FeH system. It can be rewritten in terms of the solution energy W (*c.f.* Eq. 10) as $E_{FeH} = E_{Fe} + W - \mu n$, where we have set the energy per H as $-\mu + \frac{1}{2}H_2$, in contrast with Eq. 10, where it was equal to $\frac{1}{2}E_{H_2}$.

The free energy is minimized with respect to n :

$$\frac{\delta F}{\delta n} = 0 = \frac{\partial W}{\partial n} - T \frac{\partial S}{\partial n} - \mu. \quad (25)$$

We first focus on the case of a hydrostatic strain field. For simplicity we truncate Equation 20 from the previous section to linear order in strain:

$$W \equiv W(\epsilon) = n(\Delta E - 3B^0 \Delta V \epsilon). \quad (26)$$

The expression for the entropy can take on various forms, in the presence of various forms of H-H interactions, all equivalent at lower concentrations. In what follows, n is the number of H, N_0 is the number of matrix (Fe) atoms, $N = 6N_0$ is the total number of tetrahedral interstitial lattice sites, and c is the occupation concentration defined as $c = n/N$. The simplest form for the entropy, S_0 , arises from an unrestricted concentration of H, corresponding not to a lattice but to an ideal gas. In this case, the entropy derivative is $\frac{\partial S_0}{\partial n} = -k \ln \frac{n}{N}$. The concentration yielded by Eq. 25 for the case of hydrostatic strain up to linear order in the strain takes the Maxwell-Boltzmann form of

$$c = c_0 \exp [3B^0 \Delta V \epsilon / kT]$$

where $c_0 \equiv \exp [(-\Delta E + \mu) / kT]$. This reproduces the result from the Cottrell picture of enhanced concentration around a dislocation¹¹. A more realistic form of the entropy takes into account the presence of a lattice and enforces a maximum occupancy of one H per tetrahedral site. In this case the entropy is $S_1 = -k \left[n \ln \frac{n}{N} + (N - n) \ln \left(1 - \frac{n}{N} \right) \right]$ and the entropy derivative is $\frac{\partial S_1}{\partial n} = -k \ln \frac{n}{N-n}$. The concentration using this form follows Fermi-Dirac statistics:

$$c = \left\{ \exp \left[\Delta E - \mu - 3B^0 \Delta V \epsilon / kT \right] + 1 \right\}^{-1}.$$

However, the maximum occupancy of one H per tetrahedral site is not realistic as the H-H interaction in Fe is repulsive. We have calculated the H-H interaction as a function of distance and find strong H-H repulsion up to third-nearest neighbours. For a realistic representation of the statistics, up to and including third nearest-neighbour H-H spacings should be strongly unfavourable in our model. In the extreme case, these sites are left unoccupied, corresponding to infinite repulsion. The expression for the entropy derivative for tetrahedral interstitials in a bcc lattice with total exclusion of first nearest-neighbours, both first and second-nearest-neighbours, and up to third-nearest neighbours is given by Boureau⁴⁶ as $\frac{\partial S_{1nn}}{\partial n} = -k \ln \frac{6n}{z(n+ Nz)}$ where $z = \frac{(n-3N)(5n^2-36nN+72N^2)}{(n-6N)^2 N}$, $\frac{\partial S_{2nn}}{\partial n} = -k \ln \frac{n(N-n)}{(N-4n)^2}$, and $\frac{\partial S_{3nn}}{\partial n} = -k \ln \left[\frac{n(N-3n)(N-2n)^3}{(N-4n)(N-5n)^4} \right]$ respectively. In the limits of low concentration, all of the expressions for the entropy ($S_0, S_1, S_{1nn}, S_{2nn}, S_{3nn}$) are the same, the differences being of $O(c^2)$. Similarly, at small strains, all of the solutions for c are identical.

A numerical example of the extent of the modification of the H-concentration in bcc Fe by applied hydrostatic strain is shown in Figure 13a. In this low-concentration regime, all forms of the entropy are identical. In this example, the background (zero-strain) concentration

was taken to be equal to 3×10^{-6} , in line with typical densities of H in iron². At each temperature studied, μ was adjusted in order to achieve this background concentration. From the figure, it is clear that the H-concentration can be dramatically increased by orders of magnitude, even at very small strains. This increase in concentration is more pronounced at lower temperatures, in agreement with the low thermal desorption temperatures, *ca* 400 K, indicated for H trapped at dislocations¹². Edge dislocations have a significant hydrostatic strain component⁴³ so we take our results to be representative of these. With shear strain oriented in the plane normal to the $\langle 111 \rangle$ direction, we obtain the curves in Fig. 13b. The effect is not as dramatic, because the solubility energy is quadratic in the shear strain (*c.f.* Eq. 22, whose coefficients change upon rotation to this coordinate system, but not the functional form).

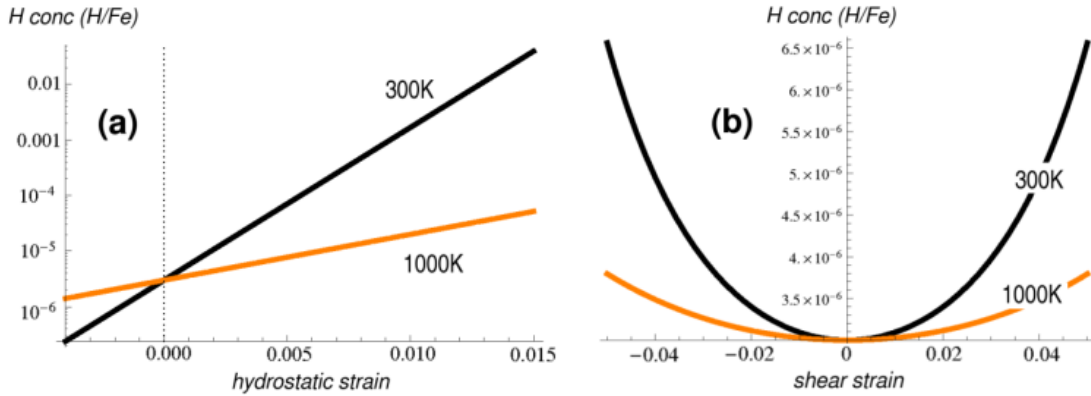


FIG. 13: Concentration of H as a function of (a) hydrostatic strain, and (b) shear strain in the plane normal to the $\langle 111 \rangle$ direction, for a chemical potential giving a background concentration of 3×10^{-6} H per Fe atom at each temperature.

V. CONCLUSIONS

We have studied the modification of elastic properties of H in bcc Fe. The modification quite profoundly affects the elastic moduli. Using this knowledge, we have characterised the strain-dependence for H-solubility in Fe. From our model we find, in agreement with existing experimental studies¹², that typical strain fields found near dislocations can trap lots of H. We further show that the local H-concentration may be enhanced by several

orders of magnitude near dislocations with tensile strain components, which justifies our use of concentrations in the atomic % range for our calculations. In the case of tensile strain, we find that these areas of enriched local concentration tend to occur mainly at low temperatures, in the hundreds of K, which agrees with the H-trapping energies found in the thermal desorption results of Novak. In the case of screw dislocations, we also find trapping of H if the screw dislocation is oriented along the $\langle 111 \rangle$ direction but the concentration enhancement is not as great as for the edge dislocation. Screw dislocations along $\langle 111 \rangle$ are the predominant types of dislocations in bcc metals driving plasticity⁴² and the concentration enhancement near screw dislocations does not rule out the HELP mechanism in explaining the mechanism of H-embrittlement of bcc Fe.

Acknowledgement

Thanks to Ralf Drautz and Thomas Hammerschmidt for proofreading and useful discussions.

-
- ¹ R. A. Oriani, *Corrosion* **43**, 390 (1987).
 - ² J. P. Hirth, *Metall. Trans. A* **11**, 861 (1980).
 - ³ A. R. Troiano, *Am. Soc. Met.* **52**, 54 (1960).
 - ⁴ R. A. Oriani and P. H. Josephic, *Acta Metall.* **25**, 979 (1977).
 - ⁵ M. S. Daw and M. I. Baskes, *Phys. Rev. Lett.* **50**, 1285 (1983).
 - ⁶ Y. Tateyama and T. Ohno, *ISIJ Int.* **43**, 573 (2003).
 - ⁷ Y. Tateyama and T. Ohno, *Phys. Rev. B* **67**, 174105 (2003).
 - ⁸ C. D. Beachem, *Metall. Trans. A* **3**, 437 (1972).
 - ⁹ H. K. Birnbaum and P. Sofronis, *Mat. Sci. Eng.* **A176**, 191 (1994).
 - ¹⁰ I. M. Robertson, *Eng. Frac. Mech.* **68**, 671 (2001).
 - ¹¹ A. H. Cottrell and B. A. Bilby, *Proc. Phys. Soc.* **62**, 49 (1949).
 - ¹² P. Novak, R. Yuan, B. P. Somerday, P. Sofronis, and R. O. Ritchie, *J. Mech. Phys. Solids* **58**, 206 (2010).
 - ¹³ G. Kresse and J. Hafner, *Phys. Rev. B* **48**, 13115 (1993).

- ¹⁴ G. Kresse and J. Furthmüller, *Comput. Mat. Sci.* **6**, 15 (1996).
- ¹⁵ G. Kresse and J. Furthmüller, *Phys. Rev. B* **54**, 11169 (1996).
- ¹⁶ P. Blochl, *Phys. Rev. B* **50**, 17953 (1994).
- ¹⁷ G. Kresse and D. Joubert, *Phys. Rev. B* **59**, 1758 (1999).
- ¹⁸ J. P. Perdew and Y. Wang, *Phys. Rev. B* **45**, 13244 (1991).
- ¹⁹ S. H. Vosko, L. Wilk, and M. Nusair, *Can. J. Phys.* **58**, 1200 (1980).
- ²⁰ J. P. Perdew, K. Burke, and M. Ernzerhof, *Phys. Rev. Lett.* **77**, 3865 (1996).
- ²¹ H. C. Herper, E. Hoffmann, and P. Entel, *Phys. Rev. B* **60**, 3839 (1999).
- ²² D. M. Clatterbuck, D. C. Chrzan, and J. W. Morris Jr., *Acta Mater.* **51**, 2271 (2003).
- ²³ J. A. Rayne and B. S. Chandrasekhar, *Phys. Rev.* **122**, 1714 (1961).
- ²⁴ M. Acet, H. Zahres, E. F. Wassermann, and W. Pepperhoff, *Phys. Rev. B* **49**, 6012 (1994).
- ²⁵ F. D. Murnaghan, *Proc. Natl. Acad. Sci. USA* **30**, 244 (1944).
- ²⁶ D. E. Jiang and E. A. Carter, *Phys. Rev. B* **70**, 064102 (2004).
- ²⁷ J. Sanchez, J. Fulla, C. Andrade, and P. L. de Andres, *Phys. Rev. B* **78**, 014113 (2008).
- ²⁸ M. J. Mehl, J. E. Osburn, D. A. Papaconstantopoulos, and B. M. Klein, *Phys. Rev. B* **41**, 10311 (1990).
- ²⁹ F. Birch, *Phys. Rev.* **71**, 809 (1947).
- ³⁰ D. C. Wallace, *Thermodynamics of Crystals* (Dover, 1972).
- ³¹ X. Sha and R. E. Cohen, *Phys. Rev. B* **74**, 214111 (2006).
- ³² K. Caspersen, A. Lew, M. Ortiz, and E. A. Carter, *Phys. Rev. Lett.* **93**, 115501 (2004).
- ³³ L. Vocadlo, G. A. de Wijs, G. Kresse, M. Gillan, and G. D. Price, *Faraday Discuss.* **106**, 205 (1997).
- ³⁴ H. Ma, S. L. Qiu, and P. M. Marcus, *Phys. Rev. B* **66**, 024113 (2002).
- ³⁵ J. J. Adams, D. S. Agosta, R. G. Leisure, and H. Ledbetter, *J. App. Phys.* **100**, 113530 (2006).
- ³⁶ S. Taketomi, R. Matsumoto, and N. Miyazaki, *Int. J. Mech. Sci.* **52**, 334 (2010).
- ³⁷ R. Hill, *J. Mech. Phys. Solids* **11**, 357 (1963).
- ³⁸ E. Lunarska, A. Zielinski, and M. Smialowski, *Acta Metall.* **25**, 305 (1977).
- ³⁹ O. Buck, L. A. Ahlberg, L. J. Graham, G. A. Alers, C. A. Wert, and K. C. Hsieh, *physica status solidi (a)* **55**, 223 (1979).
- ⁴⁰ G. R. Speich, A. J. Schwoeble, and W. C. Leslie, *Metall. Trans.* **3**, 2031 (1972).
- ⁴¹ S. Vannarat, M. H. F. Sluiter, and Y. Kawazoe, *Phys. Rev. B* **64**, 224203 (2001).

- ⁴² K. Ito and V. Vitek, *Phil. Mag. A* **81**, 1387 (2001).
- ⁴³ J. P. Hirth and J. Lothe, *Theory of Dislocations* (Krieger Pub. Co., 1992), 2nd ed.
- ⁴⁴ R. Matsumoto, Y. Inoue, S. Taketomi, and N. Miyazaki, *Scr. Mat.* **60**, 555 (2009).
- ⁴⁵ P. Sofronis and H. K. Birnbaum, *J. Mech. Phys. Solids* **43**, 49 (1995).
- ⁴⁶ G. Boureau, *J. Phys. Chem. Sol.* **42**, 743 (1981).